Title

Global Spatial and Temporal Variation of Cd:P in Euphotic Zone Particulates

Journal

Global Biogeochemical Cycles, 32(7)

ISSN

0886-6236

Authors

Bourne, HL
Bishop, JKB
Lam, PJ
et al.

Publication Date

2018-07-01

DOI

10.1029/2017gb005842

Peer reviewed

Global Spatial and Temporal Variation of Cd:P in Euphotic Zone Particulates

H. L. Bourne[1], J. K. B. Bishop[1,2], P. J. Lam[3], and D. C. Ohnemus[4]

[1] Department of Earth and Planetary Science, University of California, Berkeley, CA, USA, [2] Earth and Environmental Sciences Division, Lawrence Berkeley National Laboratory, Berkeley, CA, USA, [3] Ocean Sciences Department, University of California, Berkeley, CA, USA, [4] Bigelow Laboratory for Ocean Sciences, East Boothbay, ME, USA

Correspondence to: H. L. Bourne, hbourne@berkeley.edu

Abstract

Concentrations of Cd and P were determined in particle samples collected using the multiple unit large volume in situ filtration system (MULVFS) from 50 profiles at 34 different locations throughout the Atlantic, Pacific, and Southern Oceans since 1991. Consistent methodology has been used. This data set of Cd:P in size fractionated particles gives insight into the processes that lead to differences in regional Cd:P particle values as well as how the formation and remineralization of these particles lead to dissolved deep water ratios that increase from the North Atlantic to the North Pacific. With large spatial and temporal variation, this data set allows us to study the effects of an El Niño, upwelling, large-scale in situ Fe fertilization, low-oxygen conditions, and seasonal variation on the Cd:P in particles. Overall, Cd:P tends to be higher (~1–2 mmol/mol) in particles gathered in biologically dynamic waters and is much lower (typically ~0.1 mmol/mol) in oligotrophic regions. Using multiple linear regression analysis, we investigate how euphotic zone parameters important to photosynthesis including nitrate, phosphate, silicate, temperature, and euphotic zone depth affect the Cd:P ratio in particles. Using the results of the analysis, we create global seasonal maps of predicted particulate Cd:P distributions. We find that three factors—local dissolved nitrate, silicate concentrations, and euphotic zone depth—can predict 59% of the variation in particulate Cd:P. We verified our projections using in situ filtration samples collected during GEOTRACES expeditions GA03 (North Atlantic) and GP16 (South Pacific).

1 Introduction

Dissolved cadmium exhibits a nutrient-like profile with strong surface depletion and maximum concentrations in the 1,000- to 1,500-m-depth interval and closely follows the profile systematics of dissolved phosphate (Boyle et al., 1976; Bruland et al., 1978). Cadmium, however, is an acutely toxic element with few biological functions, while phosphate is an essential macronutrient element. The quasi-linear relationship between dissolved cadmium and phosphate and corresponding analyses of Cd:Ca ratios in the shells of benthic foraminifera in marine sediments has been used to extrapolate paleo-deep water phosphate distributions and ocean circulation

patterns of the Atlantic (Boyle, 1988). More recently, it has been used to study changes in phosphate utilization during the last glacial-interglacial in the Southern Ocean (Elderfield & Rickaby, 2000).

Although dissolved Cd has a residence time of 50,000 years, it exhibits strong biological cycling; thus, deep water Cd concentrations increase from the North Atlantic (0.3–0.4 nM) to the North Pacific (1 nM; Bruland, 1980; Bruland & Franks, 1983; John et al., 2017; Mawji et al., 2015; Xie et al., 2015). The ratio of dissolved Cd to P (units of mmol: mol) follows a parallel trend, increasing from ~0.2 in the North Atlantic to ~0.35 mmol: mol in the North Pacific (Waeles et al., 2013). These interbasin differences can be explained by an enhanced accumulation of Cd relative to P over time as deep water flows from the Atlantic to the Pacific over the thousand-year timescale of deep water circulation. Mechanistically, this could suggest regional differences in Cd:P fixation in surface waters and/or the differential remineralization of the elements from sinking particles.

Regardless of mechanism, however, the deep dissolved element pools can be presumed to represent the integrated signature of Cd:P uptake and remineralization over a great span of time. Particles, on the other hand, turn over on the timescale of 1 week in surface waters and 1 year timescales in the deeper water column (e.g., Bishop et al., 1999). Hence, direct analyses of particles allow investigation of local processes at or near to the time and location of sampling.

1.1 Mechanisms for Drivers of Particulate Cd:P Variation

The main processes driving variable Cd uptake in marine phytoplankton are not definitively known. Over the past two decades, several mechanisms have been proposed that could lead to uptake and accumulation of Cd by biota and thus its nutrient-like vertical dissolved distribution. These mechanisms can be split into two main groups: deliberate, in which Cd is actively taken up by phytoplankton for specific physiological functions, and passive bioaccumulation, generally associated with the active uptake of other bioactive trace metals. In our analysis of the spatial and seasonal differences in the Cd:P of our euphotic zone particulate samples, we explore six such mechanisms, described in detail below.

1.1.1 Passive Uptake Driven by Relative Abundance of Metals (M1)

Phytoplankton uptake of dissolved Cd has been shown to be positively correlated with free dissolved Cd (II) concentrations and inversely correlated with free dissolved Zn (II) and Mn (II) concentrations in both shipboard incubation (Cullen et al., 1999; Cullen & Sherrell, 2005) and laboratory experiments (Price & Morel, 1990; Sunda & Huntsman, 1998, 2000). This relationship likely arises from competition by these ions for cellular uptake sites (Sunda & Huntsman, 1996, 1998, 2000). It has been suggested that Cd (II) may be taken up by the same transport receptors as Fe (II); when Fe (II) levels are lower, the cell then takes up higher levels of Cd (II) (Lane et al.,

2009). Laboratory isotope site-specific fractionation experiments have shown that Cd is likely taken up passively with other divalent metals (Horner et al., 2013) and then bound within the cell to prevent toxicity. Therefore, in areas with relatively high dissolved Cd:Zn, Cd:Fe, or Cd:Mn concentrations, phytoplankton will take up more Cd.

1.1.2 Deliberate Cd Uptake Under Low-Zn Conditions (M2)

The nutrient-like profile of dissolved Cd was first attributed to abiotic processes as no biological use for Cd had been demonstrated (Price & Morel, 1990). In 1990, Price and Morel found that the diatom, *Thalassiosira weissflogii*, when grown in Zn limiting conditions, could grow at 90% of their maximum rates when supplied with Cd. Later, it was shown that marine diatoms use Cd in carbonic anhydrase (CA), an enzyme that catalyzes the formation of carbon dioxide from bicarbonate and vice versa (Lane & Morel, 2000). Xu et al. (2008) reported the crystal structure of cadmium carbonic anhydrase (CDCA1) and showed how CDCA1 is a cambialistic enzyme that can use either Zn or Cd. Therefore, substitution of Cd for Zn in diatoms for CA can relieve stress of Zn limitation (Baars et al., 2014; Lane & Morel, 2000; Lee et al., 1995; Price & Morel, 1990). This mechanism would especially affect Cd:P in regions dominated by diatoms.

1.1.3 Biodilution (M3)

Dissolved iron levels have been shown to affect uptake of Cd by phytoplankton (Cullen, 2006; Lane et al., 2009; Martin et al., 1989; Sunda & Huntsman, 2000). In HNLC regions where iron is the limiting factor in phytoplankton growth, Cd:P in phytoplankton in these regions tends to be higher than phytoplankton in iron replete conditions (Cullen, 2006; Lane et al., 2009). The higher Cd:P of phytoplankton in HNLC regions was attributed to growth rate or biodilution (Cullen, 2006; Sunda & Huntsman, 2000). In other words, while Cd uptake is relatively constant, the accumulation of biomass can vary depending on nutrient availability and growth conditions. As a result, in HNLC areas where growth is limited by iron availability, biomass and P accumulation is slower while Cd uptake is constant, leading to higher Cd:P ratios in plankton (Cullen, 2006). Oligotrophic regions, where growth is limited by macronutrients, would have lower Cd:P.

1.1.4 Species Composition (M4)

Biological variability of metal quotas of phytoplankton is large and poorly constrained. There can be great variations of P-normalized metal quotas between taxonomic groups and also between different species within a taxonomic group. There is especially high variability in Cd quotas; while other P-normalized trace metal quotas among different species were within a factor of 20, the Cd quotas for different species ranged over 2 orders of magnitude (Ho et al., 2003).

Laboratory cultures grown in nutrient replete conditions show that Cd:P content varies in different phytoplankton taxonomic groups. For example,

diatoms on average have Cd:P ratios three times lower than coccolithophores when grown in a lab in nutrient replete conditions (Finkel et al., 2007). A different culture study found in both Fe-sufficient and Fe-limited conditions that open ocean diatoms had a relatively low Cd:P compared to coccolithophores (Lane et al., 2009). The difference within the taxonomic group can be quite large as well. In the Southern Ocean, Fe-limited pennate diatoms had about 4 times lower Fe:P ratios than centric diatoms (Twining & Baines, 2013). Cyanobacteria, which likely evolved during a time of sulfidic or ferruginous oceans when Cd bioavailability would have been low, have among the lowest Cd quotas (Finkel et al., 2007; Saito et al., 2003). The differences in Cd quotas among different species, and how those species quotas change with nutrient availability can therefore affect the Cd:P in particles.

1.1.5 CdS Formation (M5)

A proposed abiotic mechanism for accumulation of particulate Cd formation is authigenic cadmium sulfide (CdS) precipitation in euxinic microenvironments of sinking aggregate particles in oxygen minimum zones (OMZ). The fragmentation of aggregates as they sink enriches the small sized particle pool with CdS particles (Janssen et al., 2014).

1.1.6 Uptake Proportional to Dissolved Concentrations (M6)

A simple mechanism, first suggested by Elderfield and Rickaby (2000), argues that preferential uptake of dissolved Cd relative to P by cells in surface waters occurs with a fractionation factor of about 2.5. Therefore, particles will be enriched in Cd:P compared to the dissolved Cd:P of surface waters. Dissolved Cd:P increases with latitude (Elderfield & Rickaby, 2000; Roshan et al., 2017). Following this mechanism, in high-latitude environments where both dissolved P and Cd:P are high, the Cd:P of particles will be high.

1.2 Systematics of Cd:P in the Ocean

Compared to the compilations of dissolved Cd profiles, published data sets of particulate Cd are few, and the ratios of Cd:P in phytoplankton have been indirectly estimated only at select sites or in laboratory cultures (Ho et al., 2003; Twining & Baines, 2013). In this study we look at the phosphorus—normalized Cd content in euphotic zone particulates collected using multiple unit large volume in situ filtration system (MULVFS) from the world's oceans (Bishop et al., 2012). We aim to quantify the wide range of cellular Cd:P in phytoplankton and to identify which of the above biotic and abiotic uptake processes may explain the observed variations. The ratio of cadmium to phosphorous was measured in 50 profiles (Table 1). The sampling has wide spatial coverage—including polar regions, and to our knowledge represent the only case of seasonal sampling over thousand-kilometer long transects. Together, these attributes allow us to study the effects of an El Niño, upwelling, large-scale in situ Fe fertilization, Zn limitation, anoxic conditions,

a phytoplankton bloom decline, and seasonal variation. By comparing at each site how euphotic zone Cd:P varies with spatial, hydrographic and biological variables such as latitude, euphotic zone depth, nitrate, phosphate, silicate, and temperature, we can evaluate whether there is a statistically significant association between these conditions and Cd versus P uptake in particles. This information is then used to predict how Cd:P varies spatially and temporally around the world. We test our empirical model by comparing particle data collected during two GEOTRACES expeditions. We also investigate how Cd:P varies in particles to kilometer depths to infer the relative lability of Cd and P.

Table 1

Table of Depth Integrated Average Measurements for All MULVFS Sites, GA03, and GP16

Station name	Date	Latitude	Longitude	Euphotic depth (m)	Euphotic temperature (°C)	Euphotic silicate (umol/kg)	Euphotic nitrate (umol/kg)	Euphotic phosphate	Euphotic Cd: P < 51 μm	Euphotic Cd: P > 51 μm
EP 3	2/8/92	9.00	−140.01	109	20.99	12.74	12.77	1.03	0.76	0.63
EP 6	2/15/92	3.00	−140.01	118	28.06	3.48	3.33	0.55	0.68	0.57
EP 8	2/21/92	1.42	−140.48	124	27.45	5.33	6.31	0.73	0.85	0.46
EP 9	2/24/92	0.00	−140.41	140	23.96	6.19	9.40	0.95	0.77	0.47
EP 10	2/27/92	−1.07	−140.30	116	27.97	2.92	5.33	0.74	0.40	0.42
EP 11	3/1/92	−1.95	−140.80	140	26.85	6.11	10.89	1.09	0.67	0.53
EP 12	3/3/92	−5.07	−140.04	124	28.06	1.88	3.38	0.51	0.37	0.51
EP 13	3/7/92	−12.03	−135.02	136	26.43	0.82	0.46	0.62	0.29	0.30
EP 16	8/11/92	12.01	−140.10	120	22.07	4.85	6.09	0.57	0.74	3.61
EP 17	8/13/92	8.97	−139.99	114	23.29	10.11	12.90	1.07	0.74	0.76
EP 18	8/17/92	7.05	−139.85	122	23.67	3.57	2.74	0.32	0.90	0.61
EP 19	8/20/92	4.95	−139.84	112	27.19	4.87	3.76	0.44	0.83	0.59
EP 20	8/22/92	2.80	−140.48	100	25.11	2.82	5.14	0.45	0.60	0.83
EP 21	8/26/92	2.10	−141.35	98	22.35	5.85	10.21	0.80	2.00	1.25
EP 22	8/27/92	1.27	−140.03	92	23.84	4.29	8.38	0.70	1.41	0.74
EP 23	8/30/92	0.33	−139.56	92	23.68	4.49	9.24	0.69	1.18	0.74
EP 24	9/1/92	−1.13	−139.98	118	22.29	5.25	10.13	0.91	1.36	0.59
EP 25	9/4/92	−2.45	−140.47	98	25.23	3.53	7.00	0.75	0.96	0.58
EP 26	9/6/92	−3.39	−140.46	108	24.90	1.69	5.75	0.47	1.04	0.69
EP 27	9/9/92	−5.35	−139.78	98	25.62	1.38	4.88	0.52	0.79	
EP 28	9/14/92	−11.85	−134.95	138	25.73	0.27	0.55	0.38	0.41	0.40
M96 OSP	3/1/96	50.00	−145.00	80	5.95	19.09	12.61	1.25	1.36	1.38
M96 P4	5/9/96	48.66	−126.67	20	10.52	7.32	1.55	0.43	0.52	
M96 P16	5/13/96	49.30	−134.70	40	8.31	9.07	6.97	0.88	0.71	0.57
M96 P20	5/16/96	49.60	−138.70	35	7.45	10.65	8.97	1.01	1.08	0.56
M96n OSP	5/19/96	50.00	−145.00	60	6.56	18.24	11.78	1.18	1.05	1.02
M96d OSP	5/21/96	50.00	−145.00	60	6.56	18.24	11.78	1.18	1.06	0.85
M96 12	5/26/96	49.00	−130.70	60	9.12	7.42	4.39	0.74	0.76	0.43
A96 P4	8/16/96	48.66	−126.67	20	14.37	3.80	0.10	0.39	0.73	0.55
A96 P12	8/19/96	49.00	−130.70	40	13.79	2.43	0.61	0.43	0.55	0.44
A96 P16	8/22/96	49.30	−134.70	40	13.08	2.15	1.17	0.48	0.46	0.38
A96 P20	8/25/96	49.60	−138.70	35	12.32	11.93	5.54	0.77	1.06	
A96n OSP	8/29/96	50.00	−145.00	40	10.44	14.67	9.26	1.03	1.38	1.30
A96d OSP	8/30/96	50.00	−145.00	40	10.44	14.67	9.26	1.03	1.67	1.34
F97 P4	2/14/97	48.66	−126.67	30	8.46	11.20	8.19	0.92	0.82	0.53
F97 P16	2/16/97	49.30	−134.70	60	7.35	12.80	8.50	0.97	0.90	0.71
F97 P12	2/24/97	49.00	−130.70	60	8.57	8.77	6.31	0.81	1.17	0.75
F97 P12	2/25/97	49.00	−130.70	60	8.57	8.77	6.31	0.81	1.10	0.72
Sofex S55 1	1/12/02	−56.50	−172.00	90	5.54	3.81	22.57	1.47	2.32	0.87
Sofex S55 2[a]	1/18/02	−55.8	−171.90	90	5.97	3.73	22.37	1.54	3.00	2.22
Sofex S66 3	1/23/02	−66.40	−171.50	60	−1.01	64.81	28.45	1.91	1.45	1.08
Sofex S66 4	1/27/02	−66.47	−171.90	60	−1.00	64.81	28.49	1.90	1.13	0.86
Sofex S66 6	2/2/02	−66.37	−171.73	60	−0.73	62.89	28.94	1.90	1.07	0.91
Sofex S66 7	2/4/02	−66.20	−172.03	45	−0.75	62.91	28.81	1.90	1.31	0.80
Sofex S55 8	2/9/02	−54.21	−169.24	60	7.52	1.06	19.74	1.30	1.32	1.26
Aloha	6/25/04	22.77	−158.00	125	24.20	1.00	0.19	0.05	0.09	0.002
K2	8/1/05	47.00	161.00	50	9.35	19.49	14.00	1.27	1.16	1.20
Bats	7/2/08	31.78	−64.10	125	20.06	0.00	0.00	0.04	0.11	0.16
Slope[a]	7/10/08	37.02	−74.41	65					0.40	0.24
Safe	5/14/09	30.00	−141.00	150	17.58	1.52	3.06	0.12	0.13	0.17
SBB[a]	5/26/09	34.27	−120.04	25					1.13	0.26
GA03 Stns.									Euphotic Cd:P 0.8–51 μm	
1	10/17/10	38.33	−9.66	61	18.712	0.708	0.031		0.10	
3	10/19/10	35.20	−16.00	103	17.974	0.787	2.000		0.32	
5	10/22/10	31.00	−21.77	118	20.219	0.568	0.187		0.15	
7	10/24/10	24.00	−22.00	110	22.988	0.847	1.689		0.16	
9	10/28/10	17.35	−18.25	82	22.096	2.448	7.828		0.36	
10	10/30/10	17.35	−20.82	80	19.896	3.554	13.415		0.34	

Table 1 *(continued)*

Station name	Date	Latitude	Longitude	Euphotic depth (m)	Euphotic temperature (°C)	Euphotic silicate (umol/kg)	Euphotic nitrate (umol/kg)	Euphotic phosphate	Euphotic Cd: P < 51 μm	Euphotic Cd: P > 51 μm
11	10/31/10	17.35	−22.78	95	21.011	2.087	7.138		0.36	
12	11/2/10	17.40	−24.50	113	21.705	1.021	4.040		0.27	
14	11/26/11	27.58	−49.63	100	22.980	0.158	0.003		0.07	
16	11/30/11	26.14	−44.83	103	23.688	0.105	0.003		0.11	
18	12/2/11	24.15	−40.22	107	24.506	0.200	0.004		0.04	
20	12/4/11	22.35	−35.87	111	23.670	0.120	0.082		0.10	
22	12/7/11	19.43	−29.38	123	23.195	0.522	1.591		0.12	
8	11/16/11	35.42	−66.54	75	22.962	0.534	0.002		0.08	
10	11/20/11	31.75	−64.17	91	22.899	0.176	0.129		0.28	
12	11/23/11	29.70	−56.82	98	23.391	0.387	0.003		0.08	
GP16 Stns.			(Independent evaluation data, not used in MLR)						Euphotic Cd:P 0.8–51 μm	
1	10/29/13	−12.0057	−79.195	61					0.57	
2	11/1/13	−12.0449	−77.376	103					1.27	
3	11/1/13	−12.045	−77.657	118					0.46	
4	11/2/13	−12.0448	−77.8182	110					1.35	
5	11/3/13	−12.0448	−78.1668	82					1.09	
7	11/5/13	−12	−83.9934	80					1.42	
9	11/8/13	−11.9993	−89.0014	95					1.23	
11	11/11/13	−12.0005	−94.0008	113					0.76	
13	11/14/13	−14	−99.0008	44					0.62	
15	11/16/13	−15.9993	−104.0005	44					0.21	
17	11/19/13	−14.9997	−109.1895	50					0.03	
18	11/21/13	−14.9835	−112.7503	49					0.14	
21	11/26/13	−14.7698	−114.9998	75					0.21	
23	11/28/13	−14.0033	−120.0022	91					0.21	
25	12/1/13	−12.5423	−124.9987	98					0.17	
26	12/3/13	−11.6703	−128.0007	100					0.23	
28	12/6/13	−11.6252	−132.5007	103					0.21	
30	12/8/13	−11.5802	−136.9804	107					0.24	
32	12/11/13	−11.0305	−142.9497	111					0.37	
34	12/14/13	−10.7654	−147.5004	123					0.27	

Note. Average Cd:P values are integrated over the euphotic zone and scaled for loss of P due to misting. Data Sources: Equatorial Pacific Nutrients: http://usjgofs.whoi.edu/jg/dir/jgofs/. K2 and ALOHA nutrients: http://ocb.whoi.edu/jg/dir/OCB/VERTIGO/. Euphotic Zone Depths from Lam et al., 2011. GA03 euphotic zone depth data is from AquaModis 8-day average euphotic zone depth data. GA03 nutrient data from IDP 2014 digital data. GA03 not used in equation (1), used in equation (2).

[a]Sites not used in linear regressions. SF55 2 is not used; only used non-Fe fertilized sites. Slope and SBB not used because nutrient data are not available.

1.3 Study Areas

MULVFS samples originating from 11 sampling campaigns are described below in chronological order of their collection (Figure 1).

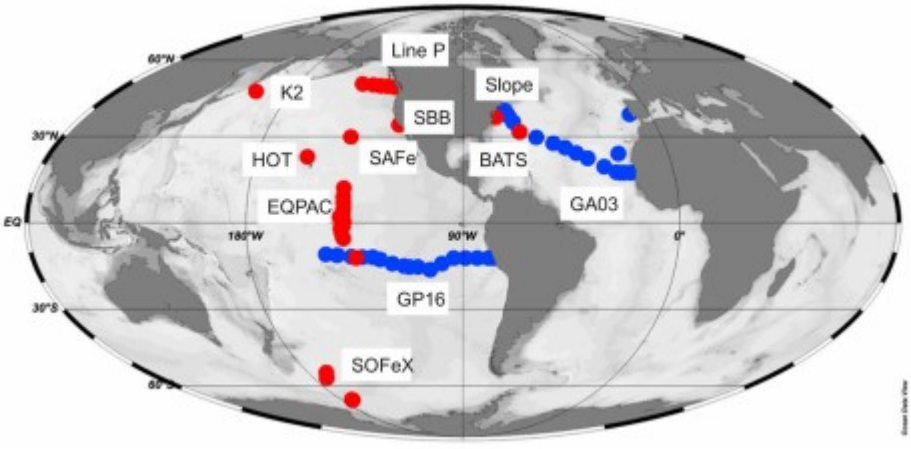

Figure 1

Map of sampling locations. MULVFS profiles are marked in red. GEOTRACES transects GA03 and GP16 (McLane samples) are marked in blue.

The equatorial Pacific (EqPac) process study of the Joint Global Ocean Flux Study (JGOFS) program from 12°N to 12°S made 21 MULVFS casts during February and August 1992 (Figure 1). The EqPac Survey I (TT007) and II (TT011) cruises captured the extremes of the 1991–1992 El Niño. Survey I samples were collected during the strong El Niño (in February of 1992), and Survey II samples were collected 6 months later during “normal” conditions (in August of 1992).

As part of the Canadian JGOFS, there were four MULVFS transects in the subarctic North Pacific from the continental slope off Vancouver Island to Ocean Station PAPA (OSP). In total, 20 MULVFS profiles were collected along Line P in February/March, June, and August 1996 and in May 1997 (Bishop et al., 1999). OSP (50°N, 145°W) has been a regularly monitored site since 1956 (Freeland, 2007).

The MULVFS was deployed during the 2001 Southern Ocean Iron Fertilization Experiment (SOFeX; Lam & Bishop, 2007). Particle samples were collected both north and south of the Antarctic polar front (APF), at 55°S and 66°S, respectively. At both locations, casts were taken prior to the addition of iron and several days subsequent to iron fertilization within the iron-fertilized patch. Control casts were also taken after fertilization from outside the iron-fertilized patch.

During the Vertical Flux in the Global Ocean (VERTIGO) project, four profiles each were collected at station ALOHA (22.75°N, 158°E), an oligotrophic station near Hawaii in June–July 2004 and at station K2 (47°N, 161°E), a biologically productive area in the Oyashio current, in July–August of 2005.

During the first GEOTRACES intercalibration cruise in June–July 2008, four MULVFS profiles were collected near the Bermuda Atlantic Time Series station (BATS 31.78°N, 64.1°W) in the oligotrophic Sargasso Sea and two profiles were made at a station in the Slope Water (37.02°N, 74.41°W) in mesotrophic waters 30 km to the west of the north wall of the Gulf Stream.

During the second GEOTRACES intercalibration cruise in May 2009, four profiles were taken at the SAFe site (37.02°N, 74.41°W) located at the edge of the oligotrophic North Pacific subtropical gyre. Two profiles were taken in the Santa Barbara Basin (34.27°N, 120.04°W), a productive regime with a strong subsurface zone of oxygen deficient water.

Particulate Cd and P measured independently on two GEOTRACES transects is then used to compare to predictions made using our MULFVS data. The two GEOTRACES transects utilized McLane pumps modified with MULVFS-style filter holders (Bishop et al., 2012). The Atlantic cruises (GA03) were collected in October/November 2010 and November/December 2011. The South Pacific cruise (GP16) was collected in November/December 2013.

2 Methods

2.1 Particulate Sampling and Analysis

The particle profiles presented in this paper were collected using the MULVFS (Bishop et al., 2012; Bishop & Wood, 2008). Briefly, the MULVFS uses a ship's electricity to power 12 pumps deployed along a 1,000-m-long electromechanical cable. Action of the pumps draws water through a filter series. The standard MULVFS filter suite consists of a 51-µm polyester mesh prefilter that is supported by a 150-µm polyester mesh, followed by two (paired) Whatman quartz microfiber filters (QMA), which are also supported by a 150-µm polyester mesh (Bishop & Wood, 2008). The three resultant size fractions from this filter suite are >51, 1–51, and <1 µm. The <1-µm fraction represents particles greater than 0.8 µm in size (Bishop et al., 2012). McLane pumps, which were used during the GEOTRACES transects GA03 and GP16, were modified according to Bishop et al. (2012) and captured >51- and 0.8- to 51-µm size fractions. The McLane 0.8- to 51-µm samples are measured on Supor filters, not QMA. The sum of 1- to 51- and <1-µm fractions from MULVFS closely mimics the 0.8- to 51-µm samples from the McLane pumps (Bishop et al., 2012).

Immediately after recovery of the MULVFS pumps from the ocean, a portion of the 1- to 51- and <1-µm QMA filters were misted with Milli Q water to aid our analyses by removing some of the salt. It was known that treatment of samples with distilled water can cause a loss of P and possibly Cd from our samples (Collier & Edmond, 1984). During the GEOTRACES 2009 intercalibration cruise, a portion of the QMA filters from each fresh sample was protected from misting using acrylic tubes to investigate the loss of labile elements. We sampled from both misted and unmisted areas of the filter from two MULVFS casts from the SAFe site.

The 1- to 51- and <1-µm QMA filters were sampled using sharpened acrylic tubes and/or stainless-steel biopsy punches. The >51-µm samples were scalpel cut using an acrylic template. Filter subsamples were then leached for 16 hr in 10 mL 0.6 N HCl solution at 60 °C. After leaching, the solution was filtered and diluted fivefold with Milli Q water then further diluted with 1% HCl and spiked with 25 ppb In before being analyzed. We used a Thermo Instruments Element II magnetic sector inductively coupled plasma mass spectrometer (ICP-MS) at Lawrence Berkeley National Laboratory (LBNL) for the majority of the samples; samples from EqPac cruises were analyzed using a VG Plasmaquad II ICP-MS. All analyses followed the same protocol described in detail by Bishop and Wood (2008). Samples were run in batches of about 70 samples per run including standards and blanks. In each run, samples were run in replicate along with several samples from previous runs. Run-to-run variability, uncertainty in blank corrections, and instrument reproducibility are included in our analysis of errors. Samples exposed at depth during MULVFS casts, but not used during filtration, were used as process blanks.

The particulate elemental concentrations in each of the three size fractions were derived by multiplying solution concentrations by the ratio of total filter area to subsample area, subtracting filter blank, and dividing by the volume of water filtered. The Cd, P, and Cd:P ratio at each sample depth was calculated, and results integrated through the euphotic zone at each site to arrive at a depth integrated average. As there was typically not a particle sample taken directly at the euphotic zone depth, values were calculated for those depths by linearly interpolating between surrounding samples.

2.1.1 Misting Experiment

No statistically significant loss or gain of Cd was found in the comparison of rinsed versus unrinsed filters collected at the SAFe station during the GEOTRACES Intercalibration Cruise II (Figure 2). In contrast, particulate P showed a small but statistically significant ~7% loss between the misted and unmisted regions of the filter. As all MULVFS samples in this study were misted, this 7% difference does not affect the systematic comparison of P concentrations. The ratios of Cd:P in our MULVFS samples as well as the misted GA03 McLane samples will differ from reality by ~7%; therefore, reported values in Table 1 have been multiplied by 1.07 to account for this effect. Most GEOTRACES data collected from GP16 with the McLane pumps were not treated with distilled water; thus, those samples are not adjusted in any way.

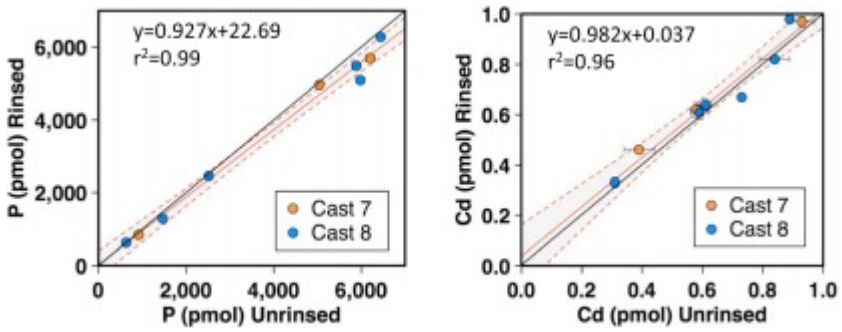

Figure 2

Comparison of rinsed (*y*-axes) and unrinsed (*x*-axes) P (left) and Cd (right) concentrations from combined 1- to 51-µm and <1-µm size fractions taken at the SAFe site. Gray shading within the dashed lines represents 95% confidence interval of a single linear regression (solid orange line). Black line is the 1:1 line. Regression for P is significantly different from the 1:1 line and shows about a 7% loss of P in rinsed samples. Regression for Cd is not statistically different from 1:1 line. Data used to create the figure can be found in Table S1.

2.2 Environmental Data

Euphotic zone depth, Z, the depth where PAR is 1% of its surface value, was calculated from surface irradiance, I_o, using the following equation:

$$Z = \ln(I_z/I_o)/-k_{PAR}$$

where Z is depth at which PAR is 1%, I_z irradiance at depth Z, I_o is irradiance at the surface, and k_{PAR} is the diffuse attenuation coefficient for PAR. Where

PAR was not measured, we used the formula, $k_{PAR} = 0.027 + c_p 0.27$, where c_p is beam attenuation coefficient derived from transmission at 660 nm (Bishop & Wood, 2009).

Dissolved phosphate, nitrate, and silicate as well as temperature for each site were downloaded from the BCO-DMO database or obtained from unpublished cruise records. Average nutrient concentrations and temperatures were calculated by integration for the euphotic zone at each site. StatPlus software package was used to perform multiple linear regression analysis of the relationships between particulate Cd:P content with latitude, euphotic zone depth, and water column euphotic zone nutrients (phosphate, nitrate, and silicate) and temperature averages. Derived simple empirical equations were used to map first-order global patterns of surface particulate Cd:P.

To create the global maps of predicted Cd:P, global profiles of objectively analyzed mean values for seasonal temperature, silicate, phosphate, and nitrate data were downloaded from the World Ocean Atlas V2 2013 in a 1° latitude/longitude grid (https://www.nodc.noaa.gov/OC5/woa13/woa13data.html). A global 1° by 1° seasonal climatology of euphotic zone depth was derived from the 9-km resolution MODIS Aqua satellite data product. In our final calculation, each grid location was used only if data for all variables was available. Our map covers approximately 90% of the ocean area (3.33×10^8 km^2 for the spring map; with area varying seasonally). The 10% loss is due to the unavailability of data in high-latitude regions in certain seasons due to seasonal ice cover and low sunlight.

3 Results and Discussion

Particulate Cd:P ratios spanned 3 orders of magnitude, from 0.01 to >2 mmol/mol, in all size fractions. There was great variability both seasonally and spatially. In order to better understand the causes of this large variability, we examine environmental conditions at each site and the potential relationship between these conditions and Cd:P. After analyzing variability in individual regions, we then examine the data set as a whole using multiple linear regression to see if we can explain local trends as part of a predictable global pattern.

3.1 Oligotrophic Versus HNLC Cd Dynamics

One of the most striking findings from the 50 locations is a marked distinction among oligotrophic, HNLC, and nutrient-replete environments. Figure 3 shows representative profiles from oligotrophic waters near Bermuda (Figure 3a), HNLC Southern Ocean waters at 55°S (Figure 3b), and nutrient replete waters of the Santa Barbara Basin (Figure 3c). Both particulate Cd and P have typical nutrient-like particle profiles in that they are relatively high at the surface where they are taken up by phytoplankton,

increase towards the chlorophyll maximum and then decrease below the euphotic zone as particles are remineralized.

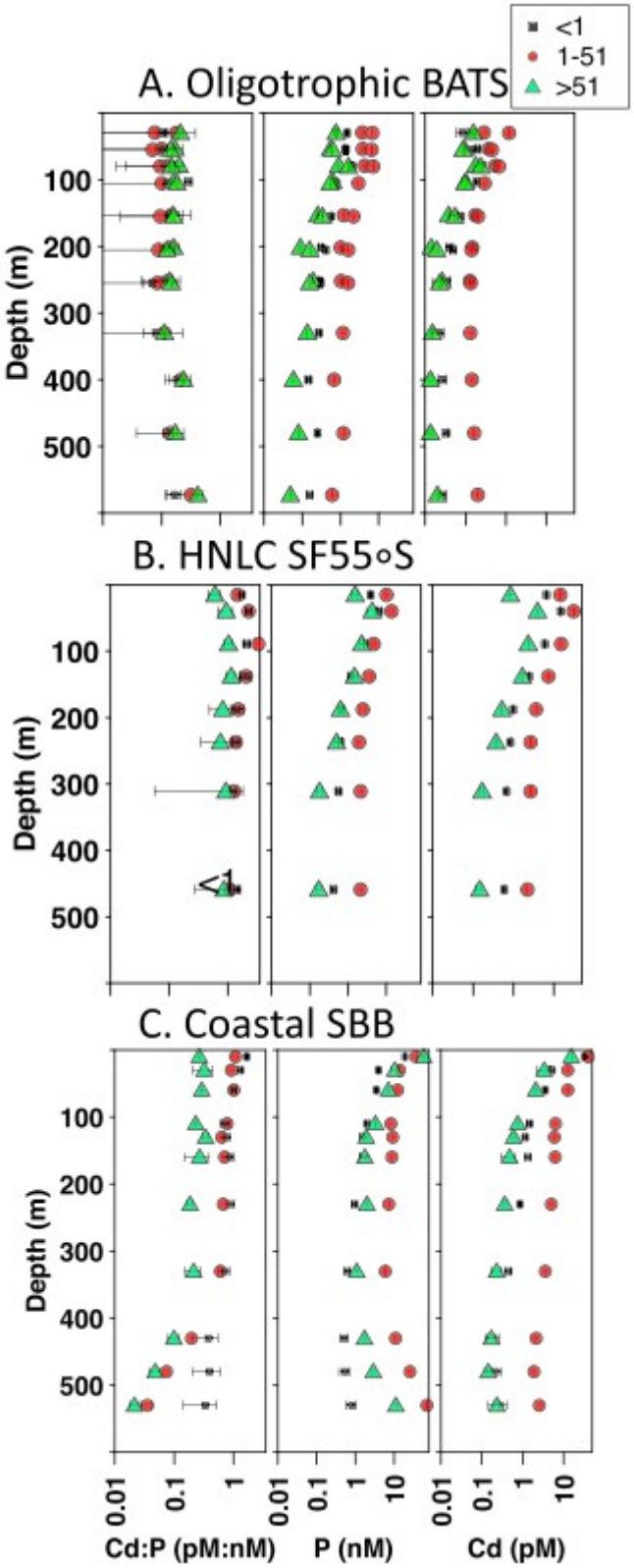
<1
1-51
>51
A. Oligotrophic BATS
B. HNLC SF55∘S
C. Coastal SBB
Depth (m)
100
200
300
400
500
0.01
0.1
1
10
Cd:P (pM:nM)
P (nM)
Cd (pM)

Figure 3

Particulate Cd:P, Cd, and P profiles from a the oligotrophic BATS site as part of the GEOTRACES Intercalibration I cruise, b 55°S in an HNLC region during the SOFEX cruise, and c the Santa Barbara Basin as part of the GEOTRACES Intercalibration II cruise, where symbols show three size fractions: >51 μm (green triangles), 1–51 μm (red circles), and <1 μm (black squares). Data used to create Figures 3a–3c can be found in Table S2–S4, respectively.

The 1- to 51-μm particulates constitute the largest amount of material of the three size fractions, and consequently, this size fraction typically has the highest concentrations of both Cd and P (Figure 3). In both the HNLC and oligotrophic profiles (Figures 3b and 3c), Cd:P is lower in the >51-μm size fraction than in the smaller size fractions. When comparing the average euphotic zone Cd:P values for the >51-μm versus the <51-μm size fractions using a paired *t* test, there is a significant difference between the two groups ($p = 0.015$). The mean Cd:P of the large size fraction is 0.2 less than the mean of the smaller particles. We focus on the <51-μm fraction due to its dominance by phytoplankton.

3.2 Remineralization of Cd Versus P

In many profiles of Cd:P ratios from open ocean upwelling environments, there is a relatively shallow subsurface maximum in Cd:P at or just below the base of the euphotic zone, seen in the compilation of profiles in Figure 4. The particulate Cd and P peaks are shallower than the Cd:P peak as seen in Figure 5. The maximum concentrations of both elements are always found in the euphotic zone. Near the euphotic zone base, particulate P concentrations decrease rapidly (Figure 5). Concentrations of Cd also decrease with depth but at a much slower rate than P. We hypothesize that this is the result of processes that preferentially remineralize P in waters shallower than ~150 m. This would agree with our misted versus nonmisted experiments where there was no significant loss of Cd from shallow samples when filters were lightly misted, but there was about a 7% loss of P. It is notable however that Cd:P decreases in waters below the Cd:P maximum implying that in the mesopelagic zone, the remaining P is less labile than Cd. This trend is seen in profiles at HNLC areas throughout the world's ocean (Figure 5).

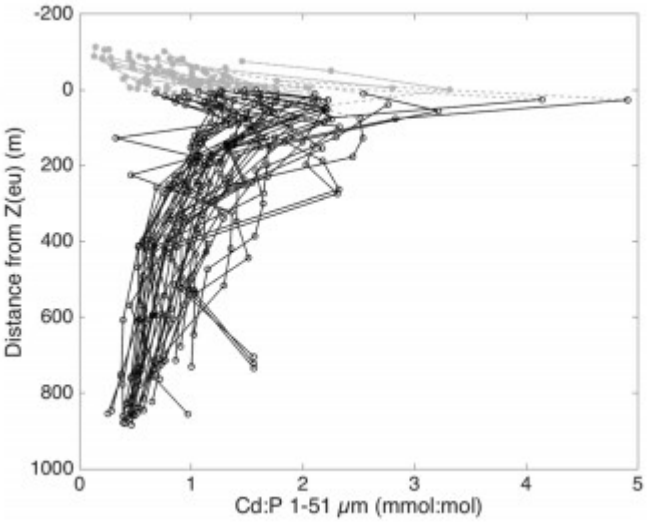

Figure 4

Overlay of all open ocean upwelling MULVFS 1- to 51-µm size fraction profiles to show trend of subsurface peaks (excludes oligotrophic sites SAFe, ALOHA, and BATS as well as the coastal anoxic Santa Barbara Basin, which show different trends). Each profile offset so that base of the euphotic zone is at 0 m. Symbols show Cd:P measurements made in the euphotic zone (light gray markers) and below the euphotic zone (black markers).

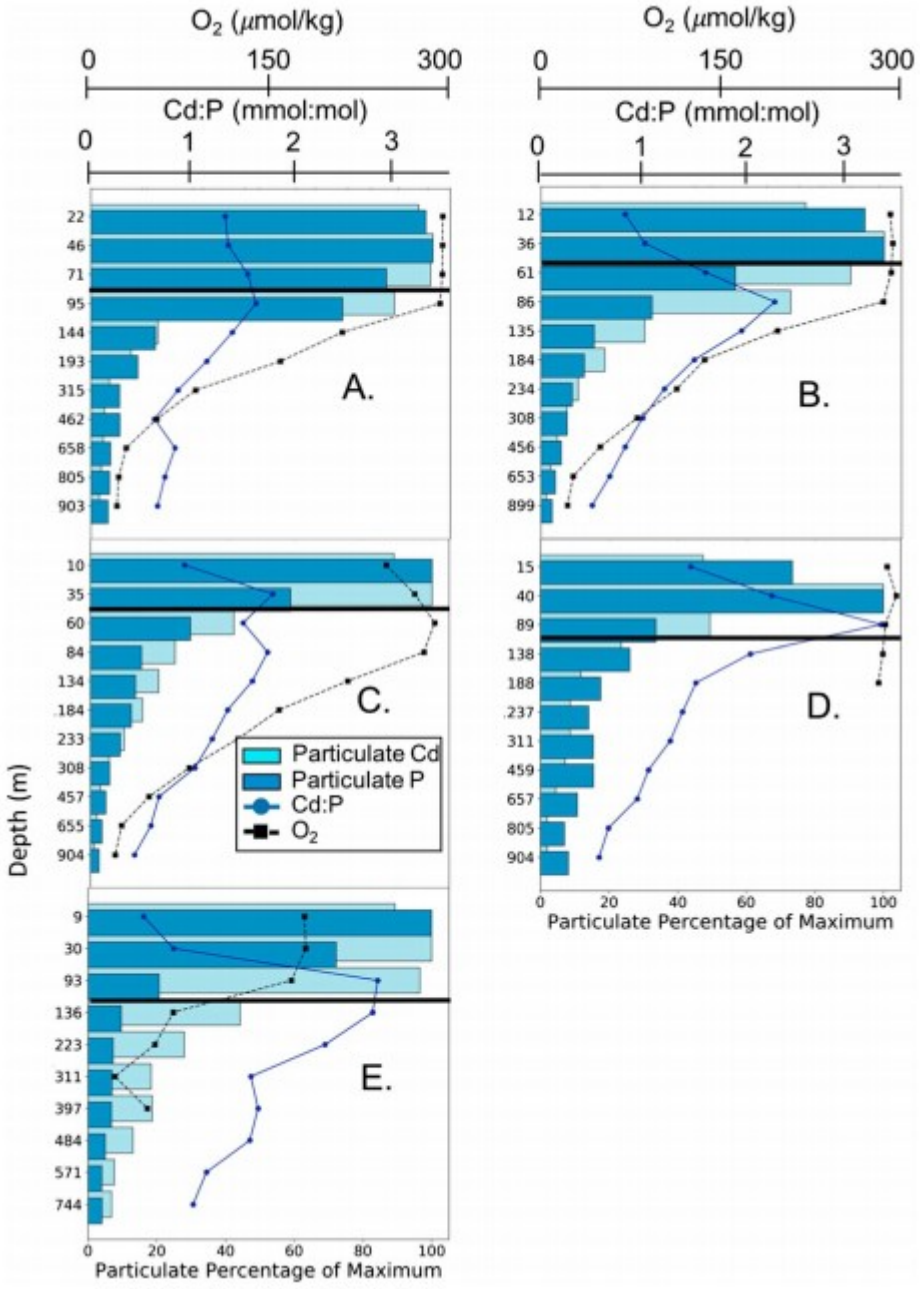

Figure 5

Particulate Cd (light blue bars) and P (dark blue bars) in the 1- to 51-µm size fraction normalized to profile-maximum values (bottom axis). Connected dashed black lines with black squares: Dissolved oxygen (top/upper axis). Connected blue dotted lines: Cd:P ratio in the 1- to 51-µm size fraction (top/lower axis). Data above thick black lines are in the euphotic zones; data below line are below euphotic zone. Data are from Ocean Station Papa on 3 March 1996 (a), 26 May 1996 (b), and 29 August 1996 (c), SOFeX at 56.5°S, 172°W on 12 January 2002 (d), and 2.1°N, 141°W on 26 August 1992 (e).

Intracellular Cd is typically bound in 4S-coordination sites in stable tetrahedral formation, such as in metallothionein and phytochelatins, which are both thought to prevent metal toxicity (Cox, 2011; Cox & Saito, 2013).

Although the function of metallothionein is still not definitively known, it may be used as an antioxidant to scavenge oxygen radicals, as a metal resistance protein for detoxifying Zn, Cd, and Cu, or for storage of excess Zn and Cu (Cox & Saito, 2013; Palmiter, 1998).

Phosphorous is located in ATP, DNA, phospholipid membranes, and others. We hypothesize that the more labile portion of bound P, such as that bound in ATP and DNA, is remineralized faster than Cd at shallow depths. The lability of Cd, we hypothesize, lies between that of the labile P and the more refractory P pool (such as phospholipids). The maximum in the Cd:P profiles, frequently observed at the base of the euphotic zone, is consistent with remineralization differences in Cd versus P in the water column (Figure 5). Differences in the remineralization rates of Cd and P could be a factor contributing to low dissolved Cd:P near the surface, and high dissolved ratios at depth in HNLC regions.

CdS crystals have been hypothesized to form in euxinic microenvironments in large aggregates as they sink due to rapid respiration rates within the aggregates (Janssen et al., 2014); these CdS particles are delivered to the small particle fraction as aggregates are broken up. Ratios of Cd:P in our profiles peak in highly oxygenated productive surface waters of the upper 100 m (Figure 5). Furthermore, dissolved oxygen begins to rapidly decline below the Cd:P particle peak. It is therefore unlikely that the precipitation of CdS crystals in euxinic microenvironments leads to these particulate Cd:P enrichments. If the Cd:P peaks were caused by authigenic formation of CdS, we would expect the gradient of oxygen loss to correspond with the particle Cd increase. No hints of this process are seen in the >51-µm fraction (Figure 3). We believe the peak Cd:P in our profiles is caused by differences in remineralization rates of Cd versus P rather than formation of CdS (M5).

3.3 Seasonal Changes

Of the 50 sites examined here, the majority of the casts come from two regions: the equatorial Pacific (21 casts) and the North-East Pacific (17 casts). These samples permitted an investigation into the effects of seasonality.

3.3.1 Line P

Between March 1996 and May 1997, the MULVFS was deployed during four expeditions along the Line P transect. The Line P transect runs from the coast of southern Vancouver Island out to ocean station PAPA (OSP: 50°N, 145°W). Macronutrient levels are never limiting along line P (Whitney & Freeland, 1999). Station 4 (48.7°N, 126.7°W) is in an Fe replete coastal region while Station PAPA is typically an HNLC region as levels of dissolved iron along Line P generally decrease from the coast out to Station PAPA. Dissolved Zn levels also decrease along the line and are extremely low at OSP (Lohan et al., 2002, 2005).

Throughout this 1-year time span, particulate Cd relative to P in the combined <1- and 1- to 51-µM size fraction varied by a factor of two at individual sites and by a factor of 3 across the transect (Figure 6a). In general, particulate Cd:P ratios increase with distance from shore, as conditions become progressively more micronutrient limited. In Fe-replete conditions closer to the coast, mean Cd:P of particles is lower. This trend supports the theory that Cd:P tends to be higher in HNLC regions due to either biodilution (M3) or by passive uptake along with other divalent metals (M1).

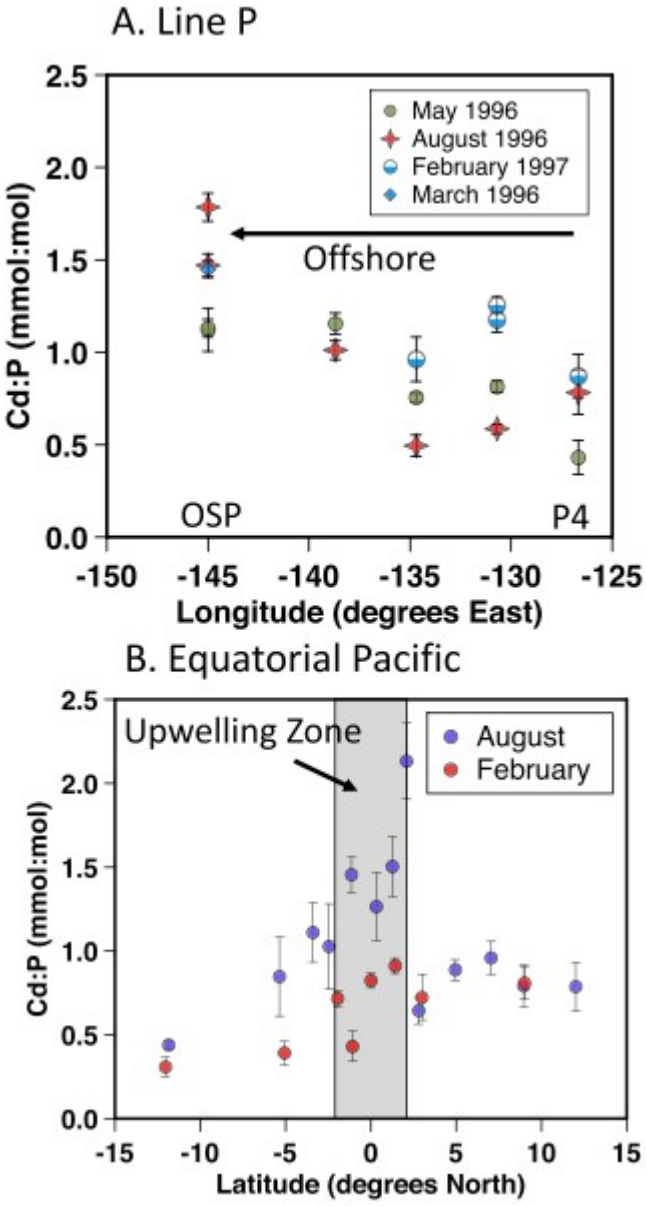

Figure 6

(a) Euphotic zone average Cd:P values in the combined <1 and the 1–51 µm size fractions along line P transect during the four cruises. Different shapes represent the different seasons. During the May and

August 1996 cruises, day and night profiles were taken at OSP (Bishop et al., 1999). Data used to create Figures 6a and 6b can be found in Tables S6 and S5, respectively.

At the time of the first MULVFS Line P cruise in February/March 1996, an iron-stimulated bloom was present at OSP. This iron likely originated from the continental margin off the Aleutian Islands (Lam & Bishop, 2008). Diatoms *Fragilariopsis* sp. and *Chaetoceros* sp. dominated the large size fraction during the February/March bloom and coccolithophores dominated the 1- to 51-µm fraction (Lam et al., 2006). Coccolithophore (*Emiliania huxleyi*) concentrations were insignificant in May (Lam et al., 2006). The February/March particulate organic carbon levels integrated to 100 m were twice as high in February/March than in May, though the surface POC levels were similar. Integrated chlorophyll levels were also twice as high in February/March than in May (Lam et al., 2006). Lam hypothesized that more bioavailable iron reached OSP in February/March than in May because the isopycnal tagged with Fe supplied from the continental shelf had outcropped at the surface early in the year and was isolated by stratification later (Lam et al., 2006). Si levels in the >51-µm fraction, from diatoms, were three times as high in March 1996 (0.22 µM) than in May and twice as high as in August.

The highest euphotic particulate Cd:P of the Line P data set is from OSP during August 1996 (Figure 6a), followed closely by OSP during February/March 1996. Though the Cd:P is very close at these two times, the environmental conditions were very different. During February/March cruise, the mixed layer and euphotic zone were approximately the same depth; during the August cruise, both the mixed layer (24 m) and euphotic layer (40 m) were far shallower than the isopycnal carrying the iron. The levels of bioavailable iron present in the euphotic zone were thus likely far lower during the August cruise than during the February/March cruise (Lam et al., 2006).

The variation in depth-integrated average euphotic Cd:P throughout these locations over three seasons is consistent with variation due to the following mechanisms: biodilution (M3), dissolved divalent metal availability leading to either specific or nonspecific uptake of Cd (M1 and M2), or community composition (M4).

3.3.2 Equatorial Pacific

The two US-JGOFS equatorial Pacific cruises in February and August 1992 allowed for the comparison of the chemistry of euphotic zone particulates during conditions of suppressed upwelling caused by an El Niño with that of normal equatorial upwelling conditions. The upwelling equatorial region is an HNLC region; two of the possible hypotheses for the low phytoplankton stocks are iron limitation and microzooplankton grazing (Chavez & Barber, 1987). During the February–March cruise, water temperatures were warmer and dissolved nutrients were lower; there was evidence of growth limitation. The sea surface temperature recorded during Survey I and II were the

warmest and coldest respectively of the JGOFS record at the time (Archer et al., 1996). The mean sea surface temperature between 10°N and 10°S was about 2° warmer during Survey I than Survey II (Archer et al., 1996). The equatorial upwelling zone is defined to be between 2°N to 2°S (Dunne et al., 1999; Murray & Leinen, 1996).

The euphotic zone particulate Cd:P in the equatorial upwelling zone during the August cruise is significantly higher (1.1 mmol: mol) than observed during the El Niño period (0.55 mmol: mol) (p = 0.006). The highest particulate Cd:P ratio (1.99 mmol: mol) was at the 2°N site during the August cruise. This station was taken in a strong frontal feature visible from space designated “the line in the sea,” which was a highly productive ocean front region (Yoder et al., 1994) associated with high abundances of the diatom *Rhizosolenia* (Yoder et al., 1994).

The observed Cd:P difference could be due to the different phytoplankton communities (M4) present during the two cruises. Very small-celled organisms, *Prochlorococcus* and *Synechococcus*, were dominant during the El Niño cruise, while diatoms were dominant during the second cruise. Diatoms are typically more sensitive to iron levels than pico-plankton and nanoplankton (Landry et al., 1995). As noted above, cyanobacteria, such as *Synechococcus* and *Prochlorococcus*, have been shown to have a lower Zn content than other phytoplankton, and an extreme Cd sensitivity (Robbins et al., 2013; Saito et al., 2003). Finkel et al. (2007) found that when grown under nutrient replete conditions, cyanobacteria have a lower Cd:P ratio than diatoms, dinoflagellates, green algae, and coccolithophorids. Cd:P of our particle samples was lower during the February–March cruise when cyanobacteria were dominant than the August–September cruise when diatoms were dominant, which is consistent with the species differences mechanism (M4) leading to differences in Cd:P uptake.

Under typical conditions, the equatorial Pacific upwelling region is growth limited by Fe and is classified as an HNLC region as there are excess macronutrients available. During El Niño conditions, when upwelling is suppressed, the region becomes more oligotrophic. The 2x-elevated Cd:P ratios observed during the regular upwelling season as opposed to the El Niño conditions could therefore also be explained as an effect of biodilution in an HNLC area (M3), preferential fractionation of Cd from high dissolved Cd:P of upwelled intermediate water leading to higher particle Cd:P (M6) or low concentrations of other divalent metals leading to an upregulation of Cd uptake (M1 and M2).

3.4 Southern Ocean

During the Southern Ocean Iron Fertilization Experiment, MULVFS casts were collected north and south of the APF, both before and following iron fertilization experiments. Both locations were iron limited; north of the APF, diatom growth was believed to be limited by silicate as concentrations (1–5 µM) were significantly lower than the levels south of the APF (>60 µM; Coale

et al., 2004). Both sites had 20-µM nitrate concentrations. Because of the silicate differences, it was hypothesized that added iron would stimulate diatoms to bloom at the 66°S site while nonsiliceous organisms would bloom at the 55°S site (Coale et al., 2004). Diatoms dominated waters at the 66°S site. At 55°S, there was a more diverse phytoplankton community with dinoflagellates and coccolithophores. Though silicate levels were low here, they were high enough to also support diatoms (Lam & Bishop, 2007). The Southern Ocean, both north and south of the APF is an HNLC environment.

Southern Ocean euphotic zone particulate Cd:P exceeded 1 mmol: mol both north and south of the APF (Table 1). The high Cd:P in the HNLC environments both north and south of the APF could, as in the case of OSP and the upwelling equatorial Pacific HNLC regions, be due to biodilution (M3) or low concentrations of divalent metals leading to an upregulation of Cd either specifically targeted or taken up obligatorily (M1 and M2).

The highest particulate Cd:P was at 55°S, north of the APF. This was true for both the >51- and <51-µm size fractions (Table 1). Along with dissolved Si concentrations, Zn concentrations are typically higher south of the polar front. In a Southern Ocean cruise in 2008, Croot et al. (2011) found that Zn concentrations in the upper 200 m south of the APF were always greater than 1 nM whereas the lowest Zn concentration was found north of the APF (0.21 nM); they also found a significant correlation between Si and Zn. Low concentrations of dissolved Zn at the 55°S site could lead to increased Cd uptake (M1).

Modeled dissolved Cd in the Southern Ocean increases across the polar front zone to higher latitudes (Roshan et al., 2017). Actual dissolved Cd:P ratios in surface waters also similarly increase (Elderfield & Rickaby, 2000). The fact that our particulate Cd:P concentrations peak at the 55°S and decrease to 66°S argues against Cd:P being purely driven by proportional uptake to dissolved Cd (M6). It is likely that in this location, the low concentrations of dissolved Zn north of the APF lead to higher particle Cd:P than south of the APF.

3.5 Global View

Cullen and Maldonado (2013) estimated surface particulate Cd:P based on analysis of the gradient of dissolved Cd and P concentrations in the nutricline at the numerous locations where both elements have been measured. They predicted particulate Cd:P ratios ranging from 0.09 to 1.9 mmol/mol. In this case, they defined HNLC conditions as stations having an annual average surface phosphate above 0.3 µM. Results gave particulate Cd:P in oligotropic and HNLC regions as 0.24 and 0.54 mmol/mol respectively. More recently, Quay et al. (2015) augmented these calculations with recent GEOTRACES and CLIVAR cruises yielding a revised particulate Cd:P for oligotrophic and HNLC regions of 0.21 ± 0.09 and 0.49 ± 0.23 mmol/mol, respectively.

In our particulate data, euphotic zone particles for the combined 1- to 51- and the <1-µm size fraction Cd:P ranged from 0.09 to 3.0 mmol: mol (Table 1). The lowest ratio was found at oligotrophic station ALOHA (0.09), while the highest value was found in the Southern Ocean at 55°S (3.0) in particles collected 6 days after the iron fertilization event. It must be noted that while collection for this cast began within the Fe fertilized patch, the ship drifted outside the fertilized region for much of the pumping, so this may represent an iron limited sample. The highest Cd:P ratio found in purely nonfertilized conditions was 2.32, also at 55°S and the second highest in upwelling equatorial Pacific waters at EP20 (2.00). In the >51-µm size fraction, the lowest Cd:P ratio was found at the oligotrophic station BATS (0.16) and the highest ratio was found at EP16 (3.61), and the second highest at 55°S (2.22) in particles collected in 6-day-old iron amended waters (Table 1).

Particulate Cd:P for oligotrophic and HNCL regimes (following Cullen & Maldonado, 2013) was 0.11 ± 0.02 (1 s.d.) and 0.98 ± 0.42, respectively. Only three of our stations had average euphotic zone phosphate concentrations less than 0.3 µmol/kg. The majority of our sites were therefore classified as not oligotrophic.

The two GEOTRACES cruises GA03 and GP16 in the North Atlantic and South Pacific, respectively, are used below as an independent point of comparison of our results and greatly expands the number of oligotrophic sites with Cd:P particulate data. The sites in the North Atlantic gyre had low surface Cd:P ratios compared to the South Pacific GP16 cruise (Table 1). The North Atlantic transect had lower nitrate levels than the South Pacific transect, which skirted the southern boundary of the Eastern Pacific equatorial upwelling region, consistent with the trend of lower Cd:P in oligotrophic regions (M3). Further, the North Atlantic transect had higher dissolved Zn and Mn levels than the South Pacific transect (Hatta et al., 2014; Resing et al., 2015). If Zn and Mn share a divalent metal transporter with Cd, the higher levels of Zn and Mn in the North Atlantic could therefore have suppressed the uptake of Cd (M1), explaining the lower Cd:P.

3.6 Linear and Multiple Linear Regressions

Linear regressions were calculated using Cd:P ratios using the combined <1- and 1- to 51-µm MULFVS fractions. Cd:P was scaled to correct for the 7% phosphorus loss from misting as described in section 2. All data used in the regression are shown in Table 1. The euphotic depth used for each sample is the depth where PAR is 1% of the surface value during the day of sampling. With each variable treated independently, the most significant relationship was between particulate Cd:P and euphotic zone phosphate (p = 2.19E−6, r^2 = 0.38), closely followed by Cd:P and euphotic zone nitrate (p = 3.60E−6, r^2 = 0.36). Relationships between particulate Cd:P and euphotic zone temperature (p = 0.00188, r^2 = 0.17), euphotic zone depth (p = 0.01624, r^2 = 0.10), and euphotic zone silicate (p = 0.0233, r^2 = 0.09) were also significant.

Multiple linear regressions were calculated with Cd:P ratio from the MULVFS data set as the independent variable and the hydrographic and nutrient data as independent variables. By comparing the adjusted r^2 values of different variable combinations, we found the best prediction of Cd:P variation:

$$Cd:P = 0.8917 - \left(0.0041^{*}Z_{(eu)}\right) - \left(.0216^{*}Si_{(eu)}\right) + \left(.0703^{*}NO_{3(eu)}\right) \quad (1)$$

where eu denotes euphotic zone.

The adjusted r^2 for this equation was 0.56. The range of independent variables used in the MLR can be seen in Figure 7. The magnitude of the contribution of euphotic zone depth (depths ranged from 20 to 150 m; Table 1) to Cd:P is −0.08 to −0.60; similarly, contributions of Si (range 0–65 μmol/Kg) are from 0 to −1.4. Both the increase of euphotic depth and Si concentrations lead to lower Cd:P ratios. In contrast, increases in NO_3 (range 0–29 μmol/kg) leads to an increase in Cd:P, with a proportional contribution to Cd:P ratio ranging from 0 to 2.0.

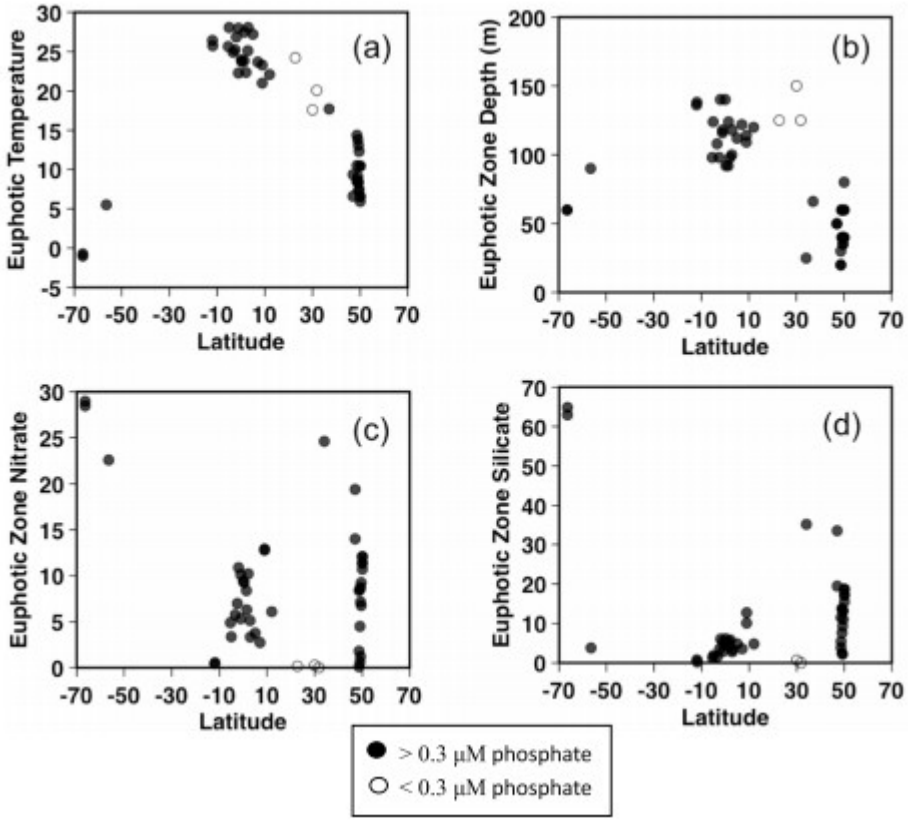

Figure 7

Average euphotic silicate (a), nitrate (b), temperature (c) and euphotic zone (d) depth versus latitude at MULVFS sites. Open circles represent waters with <0.3-μM surface dissolved phosphate; filled in circles >0.3-μM surface dissolved phosphate. Data used to create Figure 7can be found in Table S7.

Equation 1 was used to predict seasonal global euphotic zone particulate Cd:P using the 1° × 1° gridded euphotic zone depth, nitrate, and silicate data

(section 2.2) and mapped in Figure 8. The 50 MULVFS data points are also overlain on the maps for their respective seasons. We then compared our seasonal particulate predictions with independently collected particulate Cd:P data from GEOTRACES cruises, which were not used in creating the multiple linear regression. Those data points are shown overlaying the global maps in Figure 9 (September, October, and November panel). As mentioned above, the GEOTRACES 2013 transect (GP16) in the southeast Pacific and the 2010/2011 North Atlantic transect (GA03; Figure 1) were collected using McLane pumps (Lee et al., 2018; Ohnemus & Lam, 2015). Though the global map predicted general trends (Figure 9), there are some notable differences. For one, in the Autumn transect in the North Atlantic, all the McLane particulate data had lower Cd:P values than the map based on equation 1. One reason for the data-model difference is that we had far more nutrient-replete stations than oligotrophic stations in our MULVFS data set. To see if having more oligotrophic stations in our data would improve the Cd:P prediction for oligotrophic regions, we added in the sites from the North Atlantic GEOTRACES GA03 cruise and recalculated the regression. When these stations were added, the r^2 of the model increased to 0.59 with the new model better capturing Cd:P ratios in oligotrophic environments (Figure 9).

$$\mathrm{Cd:P} = 0.7629 - \left(0.0041^{*}\mathrm{Z}_{(eu)}\right) - \left(.0192^{*}\mathrm{Si}_{(eu)}\right) + \left(.0722^{*}\mathrm{NO}_{3(eu)}\right) \quad (2)$$

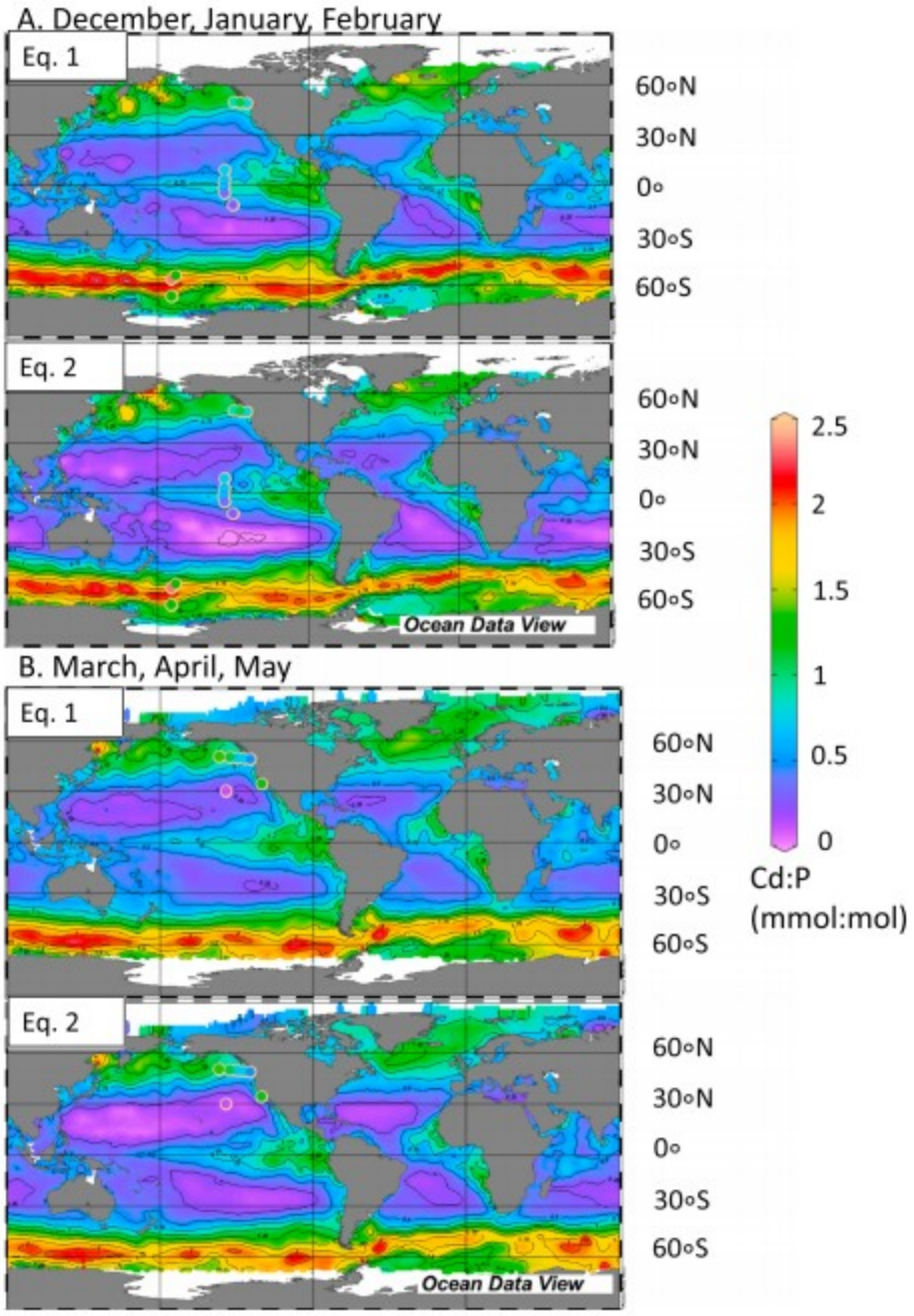
A. December, January, February
Eq. 1
60◦N
30◦N
0◦
30◦S
60◦S
Eq. 2
60◦N
30◦N
0◦
30◦S
60◦S
Ocean Data View
B. March, April, May
Eq. 1
60◦N
30◦N
0◦
30◦S
60◦S
Eq. 2
60◦N
30◦N
0◦
30◦S
60◦S
Ocean Data View
2.5
2
1.5
1
0.5
0
Cd:P
(mmol:mol)

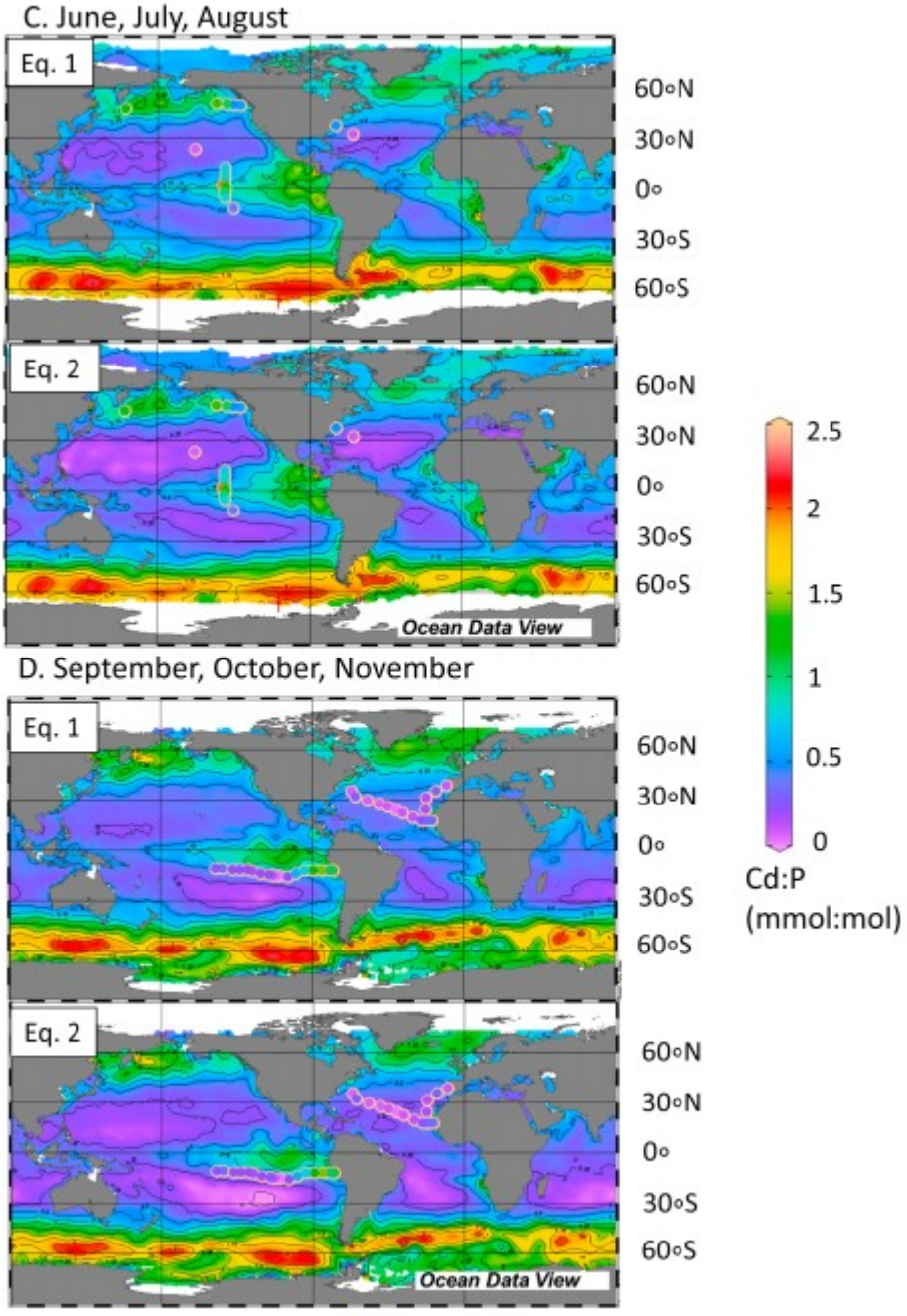

Figure 8. (continued)

Figure 8

Seasonal euphotic zone predictions of particulate Cd:P from equations 1 and 2. The predicted maps are overlain with actual euphotic zone depth integrated average Cd:P data from the seasons they were collected during. The overlain data comes both from the MULVFS casts and the GEOTRACES McLane pump casts. The South Pacific transect in (D) is independent data not used in the creation of equations 1 or 2.

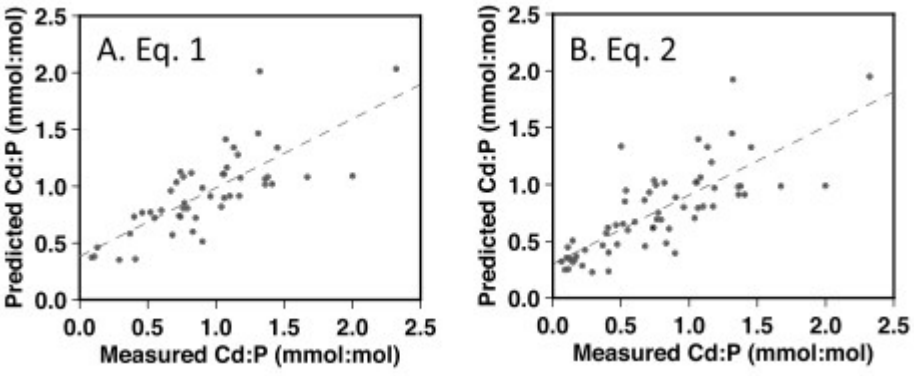

Figure 9

Regressions of actual to predicted euphotic zone Cd:P < 51-□m particles for equations 1 (a) and 2 (b). Statistics for regression shown in Table 1.

Inclusion of the GA03 results led to a 0.13 decrease of the intercept. Weighting for euphotic zone depth, Si, and NO_3 was changed slightly. Statistics for equations 1 and 2 are shown in Table 2 and regression shown in Figure 9.

Table 2
Multiple Linear Regression Statistics for Equations (1) and (2)

	Equation (1)		Adjusted R-square: 0.56		Equation (2)		Adjusted R-square: 0.59	
	Coefficient	Standard error	*p* level	H0 (5%)	Coefficient	Standard error	*p* level	H0 (5%)
Intercept	0.892	0.132	<0.001	rejected	0.763	0.132	<0.001	rejected
Euphotic Depth (m)	−0.004	0.001	0.002	rejected	−0.004	0.001	0.002	rejected
Euphotic Silicate (μmol/kg)	−0.022	0.005	<0.001	rejected	−0.019	0.005	<0.001	rejected
Euphotic Nitrate (μmol/kg)	0.07	0.010	<0.001	rejected	0.072	0.010	<0.001	rejected

Note. Regression plot shown in Figure 9.

We note that there will be some departure of our instantaneous observations compared to decadal averaged fields used for the maps. For example, effects of ENSO are averaged in WOA13 V2 data but seen in our results.

3.7 Why Do Hydrographic Variables Predict Cd:P?

Over the past four decades, there have been a number of proposals to explain why Cd:P ratios vary in dissolved profiles throughout the oceans (section 1.1). Using multiple linear regression techniques, we are able to describe ~59% of the variance of Cd uptake of particles in the euphotic zone using variables that are known to be important parameters governing phytosynthesis such as dissolved nitrate, silicate, and euphotic zone depth. Using these variables, which are broadly available and have higher spatial and temporal resolution than particulate data, we are able to make predictions of how global particulate Cd:P varies spatially during different seasons. This exercise allows us to examine, which of these parameters exert the greatest control on Cd uptake. Our statistical model used to predict Cd:P variation provides insights towards a mechanistic understanding of what processes cause this variation.

We found that the single strongest predictors of euphotic zone Cd:P were macronutrient nitrate and phosphate concentrations. In the MLR, higher nitrate concentrations drive higher particulate Cd:P ratios. High macronutrients are likely to indicate low Fe or another limiting trace metal, which would support either biodilution (M3), dissolved divalent metal availability leading to passive, or active uptake of Cd (M1 and M2). This finding supports previous field and lab studies that show variation of Cd uptake in phytoplankton with varying nutrient limitation.

In contrast, higher concentrations of dissolved Si drive particulate Cd:P lower. As Zn and Si are typically well correlated (Wyatt et al., 2014), Si may be a proxy for Zn. This supports the theory of dissolved divalent metal availability driving Cd:P differences (M1 and M2). Deeper euphotic zone depths led to lower Cd:P ratios in the MLR. Euphotic depths are typically deepest in oligotrophic gyres, which is where we found our lowest Cd:P ratios.

Macronutrients are therefore proxies for trace element concentrations that affect two of the key hypotheses for regulation of particulate Cd:P: biodilution (M3) and dissolved divalent metal availability (M1 and M2).

4 Conclusions

Since the mid-1990s, it has been noted that there must be a mechanism that preferentially removes Cd relative to phosphate in the surface ocean (Boyle, 1988). Evidence from our observations of particulate Cd and P concentrations in MULVFS profiles as well as from our misted versus unmisted filter experiments support the hypothesis that P occurs in two forms with different labilities. One phase, for example, phosphorus bound in ATP and DNA, is more labile than Cd whereas the second phase, such as phosphorus in phospholipids, is less labile than Cd. The Cd:P exported out of the euphotic zone at these sites has a higher ratio due in part to these remineralization differences. This finding is consistent with a previous study by Waeles et al. (2016) who investigated the systematics of both dissolved and particulate Cd and P off the coast of Morocco. These differences in remineralization rates would be a factor contributing to low dissolved Cd:P at the surface and high dissolved Cd:P ratios at depth in HNLC regions. We hypothesize that it is these differences in remineralization rates, rather than formation of CdS, that lead to subsurface particulate Cd:P peaks.

We see seasonal and spatial variation over an order of magnitude in particulate Cd:P ratios. In previous studies, it has both been found and predicted that particles from HNLC regions would have higher Cd:P ratios (Cullen, 2006; Lane et al., 2009). Cd:P in HNLC environments from our study also had a much higher Cd:P than particles from oligotrophic regions. Our data support the mechanisms that under Fe limitation, slower growth rates can lead to higher Cd:P (M3) and that low concentrations of dissolved Fe, Zn, and Mn can lead to increased uptake of Cd (M1 and M2). While M6 (the differential uptake of Cd and P driven by availability) would explain first-

order variations we observe, this mechanism does not hold in all locations, especially the Southern Ocean. We do not have associated dissolved trace metal data for Cd and other divalent metals such as Zn and Fe (II) at our stations. Future work examining the relationship between dissolved and particulate trace metal: P would allow for further insight into the roles of the six mechanisms.

Examining variation of these 50 casts has helped to better understand the range in particulate Cd:P both seasonally and spatially and form a predictive framework for further analysis and experimentation. This first global collection of euphotic zone Cd:P in particles follows trends predicted in previous studies and found in regionally localized studies. The contribution of this work is that we found direct links to parameters important to phytoplankton production (nitrate and silicate concentrations and euphotic zone depth) that can be used to predict broad patterns in Cd:P uptake. In understanding variation in the modern day, we can better understand what factors may have impacted Cd:P distribution in the past.

Acknowledgments

We would like to thank Todd Wood for his work both at sea and in the laboratory on the entire sample set, Louis Claxton for his help collecting and processing remote sensing data from NASA Ocean Color and Seth John for insightful comments during the review process. The MULVFS particulate sampling was supported by NSF OCE grants 0826335, 0826514, and 0930064 (GEOTRACES); NSF OCE 9022308 (EqPac); and NSERC Canada (LineP) to J. K. B. B. Hannah Bourne was supported by UC Berkeley McCone funds. NAZT GA03 was funded by OCE-0963026, and EPZT GP16 was funded by OCE-1ata518110. We thank the captains and crews of R/V Thompson, CCGS Tully, R/V Knorr, R/V Revelle, R/V Melville, and R/V Kilo Moana for their assistance at sea. The following large, publicly available data sets used in this study and how to access them are listed below. Nutrient and CTD data for the JGOFS equatorial Pacific Transects TT007 and TT011 are found: http://usjgofs.whoi.edu/jg/dir/jgofs/. Nutrient and CTD data for the VERTIGO cruises can be found: http://ocb.whoi.edu/jg/dir/OCB/VERTIGO/. Objectively analyzed climatology one degree gridded global nutrient and temperature data used in model can be found here: https://www.nodc.noaa.gov/OC5/woa13/woa13data.html. Seasonal climatology and 8-day Euphotic Zone depth averages in 9-km grid from Aqua Modis satellite can be found here: https://oceancolor.gsfc.nasa.gov/cgi/l3. Nutrient and CTD data for the GEOTRACES North Atlantic Transect can be found: https://www.bco-dmo.org/project/2066. CTD data for Line P transects are available here: http://www.waterproperties.ca/linep/. Nutrient and CTD data for SoFeX can be found: https://www.bco-dmo.org/project/2046.

References

Archer, D. E., Takahashi, T., Sutherland, S., Goddard, J., Chipman, D., Rodgers, K., & Ogura, H. (1996). Daily, seasonal and interannual variability of

sea-surface carbon and nutrient concentration in the equatorial Pacific Ocean. *Deep Sea Research Part II: Topical Studies in Oceanography*, 43(4-6), 779– 808. https://doi.org/10.1016/0967-0645(96)00017-3

Baars, O., Abouchami, W., Galer, S., Boye, M., & Croot, P. (2014). Dissolved cadmium in the Southern Ocean: Distribution, speciation, and relation to phosphate. *Limnology and Oceanography*, 59(2), 385– 399. https://doi.org/10.4319/lo.2014.59.2.0385

Bishop, J. K. B., Calvert, S. E., & Soon, M. Y. S. (1999). Spatial and temporal variability of POC in the northeast subarctic Pacific. *Deep Sea Research Part II: Topical Studies in Oceanography*, 46(11–12), 2699– 2733. https://doi.org/10.1016/S0967-0645(99)00081-8

Bishop, J. K. B., Lam, P. J., & Wood, T. J. (2012). Getting good particles: Accurate sampling of particles by large volume in-situ filtration. *Limnology and Oceanography: Methods*, 10, 681– 710. https://doi.org/10.4319/lom.2012.10.681

Bishop, J. K. B., & Wood, T. J. (2008). Particulate matter chemistry and dynamics in the twilight zone at VERTIGO ALOHA and K2 sites. *Deep-Sea Research Part I: Oceanographic Research Papers*, 55(12), 1684– 1706. https://doi.org/10.1016/j.dsr.2008.07.012

Bishop, J. K. B., & Wood, T. J. (2009). Year-round observations of carbon biomass and flux variability in the Southern Ocean. *Global Biogeochemical Cycles*, 23, GB2019. https://doi.org/10.1029/2008GB003206

Boyle, E. A. (1988). Cadmium: Chemical tracer of deepwater paleoceanography. *Paleoceanography*, 3(4), 471– 489. https://doi.org/10.1029/PA003i004p00471

Boyle, E. A., Sclater, F., & Edmund, J. M. (1976). On the marine geochemistry of cadmium. *Nature*, 263(5572), 42– 44. https://doi.org/10.1038/263042a0

Bruland, K. W. (1980). Oceanographic distribution of cadmium, zinc, nickel and copper in the North Pacific. *Earth and Planetary Science Letters*, 47(2), 176– 198. https://doi.org/10.1016/0012-821X(80)90035-7

Bruland, K. W., & Franks, R. P. (1983). Trace elements in sea water. In J. P. Riley & R. Chester (Eds.), *Chemical oceanography*, (pp. 157, 8– 220). London: Academic Press.

Bruland, K. W., Knauer George, A., & Martin John, H. (1978). Cadmium in northeast Pacific waters. *Limnology and Oceanography*, 23. 618– 625. https://doi.org/10.4319/lo.1978.23.4.0618

Chavez, F. P., & Barber, R. T. (1987). An estimate of new production in the equatorial Pacific. *Deep-Sea Research*, 34(7), 1229– 1243. https://doi.org/10.1016/0198-0149(87)90073-2

Coale, K. H., Johnson, K. S., Chavez, F. P., Buesseler, K. O., Barber, R. T., Brzezinski, M. A., et al. (2004). Southern Ocean iron enrichment experiment:

Carbon cycling in high- and low-Si waters. *Science*, 304(5669), 408– 414. https://doi.org/10.1126/science.1089778

Collier, R., & Edmond, J. (1984). The trace element geochemistry of marine biogenic particulate matter. *Progress in Oceanography*, 13(2), 113– 199. https://doi.org/10.1016/0079-6611(84)90008-9

Cox, A. D. (2011). Interactions of cadmium, zinc, and phosphorus in marine Synechococcus: Field uptake, physiological and proteomic studies, Ph.D., Woods Hole Oceanographic Institution, Woods Hole MA. https://doi.org/10.1575/1912/4645

Cox, A. D., & Saito, M. a. (2013). Proteomic responses of oceanic Synechococcus WH8102 to phosphate and zinc scarcity and cadmium additions. *Frontiers in Microbiology*, 4(DEC), 1– 17. https://doi.org/10.3389/fmicb.2013.00387

Croot, P. L., Baars, O., & Streu, P. (2011). The distribution of dissolved zinc in the Atlantic sector of the Southern Ocean. *Deep Sea Research Part II: Topical Studies in Oceanography*, 58(25–26), 2707– 2719. https://doi.org/10.1016/j.dsr2.2010.10.041

Cullen, J. T. (2006). On the nonlinear relationship between dissolved cadmium and phosphate in the modern global ocean: Could chronic iron limitation of phytoplankton growth cause the kink? *Limnology and Oceanography*, 51(3), 1369– 1380. https://doi.org/10.4319/lo.2006.51.3.1369

Cullen, J. T., Lane, T. W., Morel, F. M. M., & Sherrell, R. M. (1999). Modulation of cadmium uptake in phytoplankton by seawater CO2 concentration. *Nature*, 402(6758), 165– 167. https://doi.org/10.1038/46007

Cullen, J. T., & Maldonado, M. T. (2013). Biogeochemistry of cadmium and its release to the environment. In A. Sigel, et al. (Eds.), *Cadmium: From toxicity to essentiality*, (pp. 31– 62). Dordrecht: Springer.

Cullen, J. T., & Sherrell, R. M. (2005). Effects of dissolved carbon dioxide, zinc, and manganese on the cadmium to phosphorus ratio in natural phytoplankton assemblages. *Limnology and Oceanography*, 50(4), 1193– 1204. https://doi.org/10.4319/lo.2005.50.4.1193

Dunne, J. P., Murray, J. W., & Aufdenkampe, A. K. (1999). Silicon-nitrogen coupling in the equatorial Pacific upwelling zone. *Global Biogeochemical Cycles*, 13(3), 715– 726. https://doi.org/10.1029/1999GB900031

Elderfield, H., & Rickaby, R. (2000). Oceanic Cd/P ratio and nutrient utilization in the glacial Southern Ocean. *Nature*, 405(6784), 305– 310. https://doi.org/10.1038/35012507

Finkel, Z. V., Quigg, A. S., Chiampi, R. K., Schofield, O. E., & Falkowski, P. G. (2007). Phylogenetic diversity in cadmium: Phosphorus ratio regulation by

marine phytoplankton. *Limnology and Oceanography*, 52(3), 1131– 1138. https://doi.org/10.4319/lo.2007.52.3.1131

Freeland, H. (2007). A short history of Ocean Station Papa and Line P. *Progress in Oceanography*, 75(2), 120– 125. https://doi.org/10.1016/j.pocean.2007.08.005

Hatta, M., Measures, C. I., Wu, J., Roshan, S., Fitzsimmons, J. N., Sedwick, P., & Morton, P. (2014). An overview of dissolved Fe and Mn distributions during the 2010–2011 U.S. GEOTRACES north Atlantic cruises: GEOTRACES GA03. *Deep Sea Research Part II: Topical Studies in Oceanography*, 116, 117– 129. https://doi.org/10.1016/j.dsr2.2014.07.005

Ho, T. Y., Quigg, A., Finkel, Z. V., Milligan, A. J., Wyman, K., Falkowski, P. G., & Morel, F. M. M. (2003). The elemental compostion of some marine phytoplankton. *Journal of Phycology*, 39(6), 1145– 1159. https://doi.org/10.1111/j.0022-3646.2003.03-090.x

Horner, T. J., Lee, R. B. Y., Henderson, G. M., & Rickaby, R. E. M. (2013). Nonspecific uptake and homeostasis drive the oceanic cadmium cycle. *Proceedings of the National Academy of Sciences of the United States of America*, 110(7), 2500– 2505. https://doi.org/10.1073/pnas.1213857110

Janssen, D. J., Conway, T. M., John, S. G., Christian, J. R., Kramer, D. I., Pedersen, T. F., & Cullen, J. T. (2014). Undocumented water column sink for cadmium in open ocean oxygen-deficient zones. *Proceedings of the National Academy of Sciences*, 111(19), 6888– 6893. https://doi.org/10.1073/pnas.1402388111

John, S. G., Helgoe, J., & Townsend, E. (2017). Biogeochemical cycling of Zn and Cd and their stable isotopes in the eastern tropical South Pacific. *Marine Chemistry*. https://doi.org/10.1016/j.marchem.2017.06.001

Lam, P. J., & Bishop, J. K. B. (2007). High biomass, low export regimes in the Southern Ocean. *Deep Sea Research Part II: Topical Studies in Oceanography*, 54(5–7), 601– 638. https://doi.org/10.1016/j.dsr2.2007.01.013

Lam, P. J., & Bishop, J. K. B. (2008). The continental margin is a key source of iron to the HNLC North Pacific Ocean. *Geophysical Research Letters*, 35, L07608. https://doi.org/10.1029/2008GL033294

Lam, P. J., Bishop, J. K. B., Henning, C. C., Marcus, M. a., Waychunas, G. a., & Fung, I. Y. (2006). Wintertime phytoplankton bloom in the subarctic Pacific supported by continental margin iron. *Global Biogeochemical Cycles*, 20, GB1006. https://doi.org/10.1029/2005GB002557

Lam, P. J., Doney, S. C., & Bishop, J. K. B. (2011). The dynamic ocean biological pump: Insights from a global compilation of particulate organic carbon, CaCO3, and opal concentration profiles from the mesopelagic. *Global Biogeochemical Cycles*, 25, GB3009. https://doi.org/10.1029/2010GB003868

Landry, M. R., Constantinou, J., & Kirshtein, J. (1995). Microzooplankton grazing in the central equatorial Pacific during February and August, 1992. *Deep Sea Research Part II: Topical Studies in Oceanography*, 42(2–3), 657– 671. https://doi.org/10.1016/0967-0645(95)00024-K

Lane, E. S., Semeniuk, D. M., Strzepek, R. F., Cullen, J. T., & Maldonado, M. T. (2009). Effects of iron limitation on intracellular cadmium of cultured phytoplankton: Implications for surface dissolved cadmium to phosphate ratios. *Marine Chemistry*, 115(3–4), 155– 162. https://doi.org/10.1016/j.marchem.2009.07.008

Lane, T. W., & Morel, F. M. (2000). A biological function for cadmium in marine diatoms. *Proceedings of the National Academy of Sciences of the United States of America*, 97(9), 4627– 4631. https://doi.org/10.1073/pnas.090091397

Lee, J. L., Roberts, S. B., & Morel, F. M. M. (1995). Cadmium: A nutrient for the marine diatom Thalassiosira weissflogii. *Limnology and Oceanography*, 40(6), 1056– 1063. https://doi.org/10.4319/lo.1995.40.6.1056/

Lee, J.-M., Heller, M. I., & Lam, P. J. (2018). Size distribution of particulate trace elements in the U.S. GEOTRACES Eastern Pacific Zonal Transect (GP16). *Marine Chemistry*, 201, 108– 123. https://doi.org/10.1016/j.marchem.2017.09.006

Lohan, M. C., Crawford, D. W., Purdie, D. A., & Statham, P. J. (2005). Iron and zinc enrichments in the northeastern subarctic Pacific: ligand production and zinc availability in response to phytoplankton growth. *Limnology and Oceanograhy*, 50(5), 1427– 1437. https://doi.org/10.4319/lo.2005.50.5.1427

Lohan, M. C., Statham, P. J., & Crawford, D. W. (2002). Total dissolved zinc in the upper water column of the subarctic North East Pacific. *Deep Sea Research Part II: Topical Studies in Oceanography*, 49(24–25), 5793– 5808. https://doi.org/10.1016/S0967-0645(02)00215-1

Martin, J. H., Gordon, R. M., Fitzwater, S., & Broenkow, W. W. (1989). Vertex: Phytoplankton/iron studies in the Gulf of Alaska. *Deep-Sea Research Part I: Oceanographic Research Papers*, 36(5), 649– 680. https://doi.org/10.1016/0198-0149(89)90144-1

Mawji, E., Schlitzer, R., Dodas, E. M., Abadie, C., Abouchami, W., Anderson, R. F., et al. (2015). The GEOTRACES intermediate data product 2014. *Marine Chemistry*, 177(part 1), 1– 8. https://doi.org/10.1016/j.marchem.2015.04.005

Murray, R. W., & Leinen, M. (1996). Scavenged excess aluminum and its relationship to bulk titanium in biogenic sediment from the central equatorial Pacific Ocean. *Geochimica et Cosmochimica Acta*, 60(20), 3869– 3878. https://doi.org/10.1016/0016-7037(96)00236-0

Ohnemus, D. C., & Lam, P. J. (2015). Cycling of lithogenic marine particles in the US GEOTRACES North Atlantic transect. *Deep Sea Research Part II:*

Topical Studies in Oceanography, 116, 283– 302. https://doi.org/10.1016/j.dsr2.2014.11.019

Palmiter, R. D. (1998). The elusive function of metallothioneins. *Proceedings of the National Academy of Sciences of the United States of America*, 95(15), 8428– 8430. https://doi.org/10.1073/pnas.95.15.8428

Price, N. M., & Morel, F. M. M. (1990). Cadmium and colbalt substitiutions for zinc in a marine diatom. *Nature*, 344(6267), 658– 660. https://doi.org/10.1038/344658a0

Quay, P., Cullen, J., Landing, W., & Morton, P. (2015). Processes controlling the distributions of Cd and PO4 in the ocean. *Global Biogeochemical Cycles*, 29, 830– 841. https://doi.org/10.10002/2014GB004998

Resing, J. A., Sedwick, P. N., German, C. R., Jenkins, W. J., Moffett, J. W., Sohst, B. M., & Tagliabue, A. (2015). Basin-scale transport of hydrothermal dissolved metals across the South Pacific Ocean. *Nature*, 523(7559), 200– 203. https://doi.org/10.1038/nature14577

Robbins, L. J., Lalonde, S. V., Saito, M. a., Planavsky, N. J., Mloszewska, a. M., Pecoits, E., et al. (2013). Authigenic iron oxide proxies for marine zinc over geological time and implications for eukaryotic metallome evolution. *Geobiology*, 11(4), 295– 306. https://doi.org/10.1111/gbi.12036

Roshan, S., Wu, J., & DeVries, T. (2017). Controls on the cadmium-phosphate relationship in the tropical South Pacific. *Global Biogeochemical Cycles*, 31, 1516– 1527. https://doi.org/10.1002/2016GB005556

Saito, M. a., Sigman, D. M., & Morel, F. M. M. (2003). The bioinorganic chemistry of the ancient ocean: The co-evolution of cyanobacterial metal requirements and biogeochemical cycles at the Archean-Proterozoic boundary? *Inorganica Chimica Acta*, 356, 308– 318. https://doi.org/10.1016/S0020-1693(03)00442-0

Sunda, W. G., & Huntsman, S. A. (1996). Antagonism between cadmium and zinc toxicity and manganese limitation in a coastal diatom. *Limnology and Oceanography*, 41(3), 373– 387. https://doi.org/10.4319/lo.1996.41.3.0373

Sunda, W. G., & Huntsman, S. a. (1998). Interactions among Cu2+, Zn2+, and Mn2+ in controlling cellular Mn, Zn, and growth rate in the coastal alga Chlamydomonas. *Limnology and Oceanography*, 43(6), 1055– 1064. https://doi.org/10.4319/lo.1998.43.6.1055

Sunda, W. G., & Huntsman, S. A. (2000). Effect of Zn, Mn, and Fe on Cd accumulation in phytoplankton: Implications for oceanic cd cycling. *Limnology and Oceanography*, 45(7), 1501– 1516. https://doi.org/10.4319/lo.2000.45.7.1501

Twining, B. S., & Baines, S. B. (2013). The trace metal composition of marine phytoplankton. *Annual Review of Marine Science*, 5(1), 191– 215. https://doi.org/10.1146/annurev-marine-121211-172322

Waeles, M., Maguer, J.-F., Baurand, F., & Riso, R. D. (2013). Off Congo waters (Angola Basin, Atlantic Ocean): A hot spot for cadmium-phosphate fractionation. *Limnology and Oceanography*, 58(4), 1481– 1490. https://doi.org/10.4319/lo.2013.58.4.1481

Waeles, M., Planquette, H., Afandi, I., Delebecque, N., Bouthir, F., Donval, A., et al. (2016). Cadmium in the waters off South Morocco: Nature of particles hosting Cd and insights into the mechanisms fractionating cd from phosphate. *Journal of Geophysical Research: Oceans*, 121, 3106– 3120. https://doi.org/10.1002/2016JC011688

Whitney, F. A., & Freeland, H. J. (1999). Variability in upper-ocean water properties in the NE Pacific Ocean. *Deep Sea Research*, 46(11-12), 2351– 2370. https://doi.org/10.1016/S0967-0645(99)00067-3

Wyatt, N. J., Milne, A., Woodward, E. M. S., Rees, A. P., Browning, T. J., Bouman, H. A., et al. (2014). Biogeochemical cycling of dissolved zinc along the GEOTRACES South Atlantic transect GA10 at 40°S. *Global Biogeochemical Cycles*, 28, 44– 56. https://doi.org/10.1002/2013GB004637

Xie, R. C., Galer, S. J. G., Abouchami, W., Rijkenberg, M. J. A., Jong, J. D., de Baar, H. J. W., & Andreae, M. O. (2015). The cadmium-phosphate relationship in the western South Atlantic—The importance of mode and intermediate waters on the global systematics. *Marine Chemistry*, 177, 110– 123. https://doi.org/10.1016/j.marchem.2015.06.011

Xu, Y., Feng, L., Jeffrey, P. D., Shi, Y., & Morel, F. M. M. (2008). Structure and metal exchange in the cadmium carbonic anhydrase of marine diatoms. *Nature*, 452(7183), 56– 61. https://doi.org/10.1038/nature06636

Yoder, J. A., Ackleson, S. G., Barber, R. T., Flament, P., & Balch, W. M. (1994). A line in the sea. *Nature*, 371(6499), 689– 692. https://doi.org/10.1038/371689a0